Amino Acids (2011) 41:1093–1101
DOI 10.1007/s00726-010-0515-5

ORIGINAL ARTICLE

A cell permeable peptide analog as a potential-specific PET imaging probe for prostate cancer detection

Guiyang Hao · Jian Zhou · Yi Guo · Michael A. Long · Tiffani Anthony · Jennifer Stanfield · Jer-Tsong Hsieh · Xiankai Sun

Received: 25 November 2009 / Accepted: 4 February 2010 / Published online: 11 March 2010

Abstract Non-invasive detection of prostate cancer or metastases still remains a challenge in the field of molecular imaging. In our recent work of screening arginine- or lysine-rich peptides for intracellular delivery of a therapeutic agent into prostate cancer cells, an arginine-rich cell permeable peptide (NH_2GR_{11}) was found with an unexpectedly preferential uptake in prostate cancer cell lines. The goal of this work was to develop this peptide as a positron emission tomography (PET) imaging probe for specific detection of distant prostate cancer metastases. The optimal length of arginine-rich peptides was evaluated by the cell uptake efficiency of three fluorescein isothiocyanate (FITC)-tagged oligoarginines ($NHGR_9$, $NHGR_{11}$, and $NHGR_{13}$) in four human prostate cell lines (LNCaP, PZ-HPV-7, DU145, and PC3). Of the three oligoarginines, NH_2GR_{11} showed the highest cell uptake and internalization efficiency with its subcellular localization in cytosol. The biodistribution of FITC-$NHGR_9$, FITC-$NHGR_{11}$, and FITC-$NHGR_{13}$ performed in control nude mice displayed the unique preferential accumulation of FITC-$NHGR_{11}$ in the prostate tissue. Further in vivo evaluation of FITC-$NHGR_{11}$ in PC3 tumor-bearing nude mice revealed elevated uptake of this peptide in tumors as compared to other organs. In vivo pharmacokinetics evaluated with ^{64}Cu-labeled NH_2GR_{11} showed that the peptide was rapidly cleared from the blood ($t_{1/2} = 10.7$ min) and its elimination half-life was 17.2 h. The PET imaging specificity of ^{64}Cu-labled NH_2GR_{11} was demonstrated for the detection of prostate cancer in a comparative imaging experiment using two different human cancer xenograft models.

Keywords PET · Prostate cancer · Cell permeable peptide · ^{64}Cu

G. Hao · Y. Guo · M. A. Long · T. Anthony
Department of Radiology, University of Texas Southwestern Medical Center, Dallas, TX 75390, USA

J. Zhou · J. Stanfield · J.-T. Hsieh (✉)
Department of Urology, University of Texas Southwestern Medical Center, Dallas, TX 75390, USA
e-mail: JT.Hsieh@UTSouthwestern.edu

X. Sun (✉)
Department of Radiology, Advanced Imaging Research Center, University of Texas Southwestern Medical Center, Dallas, TX 75390, USA
e-mail: Xiankai.Sun@UTSouthwestern.edu

Introduction

Currently the most commonly used positron emission tomography (PET) probe, 2-^{18}F-fluoro-2-deoxy-D-glucose (^{18}F-FDG), is not so successful at identifying localized prostate cancer or distal metastases because the prostate is in the close proximity of the bladder, where the FDG is cleared, and the prostate cancer cells are inherently not glucose avid (Shreve et al. 1996; Etchebehere et al. 2002; Gambhir 2002). To date, various PET tracers have been introduced for prostate cancer imaging based on different molecular mechanisms (Emonds et al. 2009). To name a few, ^{11}C- or ^{18}F-labeled choline showed promising results of detecting primary and metastatic prostate cancer but with inconsistent findings in densely sclerotic bone lesions (Hara et al. 1998; Maeda et al. 2006; Vees et al. 2007; Giovacchini et al. 2008); ^{11}C- or ^{18}F-labeled acetate was reported with potential to detect local recurrences and regional lymph node metastases (Oyama et al. 2002; Albrecht et al. 2007; Ponde et al. 2007); 3′-^{18}F-fluorothymidine was used for monitoring the therapeutic effect of

androgen ablation therapy in prostate cancer (Oyama et al. 2004); 16β-^{18}F-fluoro-5α-dihydrotesterone was employed to detect prostate cancer metastases and access androgen receptor expression in vivo (Larson et al. 2004); and radiolabeled peptides have been exploited for specific prostate cancer imaging by targeting specific surface markers or receptors (Rogers et al. 2003; Chen et al. 2004a, b; Schuhmacher et al. 2005; Yang et al. 2006; Zhang et al. 2006). However, the role of PET in the diagnosis of prostate cancer, either localized diseases or distal metastases, has not been established (Beheshti et al. 2009; Bouchelouche et al. 2009). Prostate cancer metastases, especially in their early stage, display the dormant characteristics of prostate cancer with relatively small size as compared to metastases of other carcinomas, such as breast and lung cancer (Fogelman et al. 2005; Langsteger et al. 2006). This represents a great challenge in the non-invasive detection of prostate cancer and its metastases. As such, it is highly desirable to develop specific PET imaging probes based on different molecular mechanisms.

Cell permeable peptides (CPPs) known as delivery vehicles that can cross cell membranes have been extensively used for intracellular delivery of varieties of bioactive cargos (Bucci et al. 2000; Gratton et al. 2003). Of the commonly used CPPs, arginine-rich CPPs including HIV-Tat peptides and oligoarginines have been reported with high internalization efficacy likely because their guanidine moiety can form divalent hydrogen-bonds with phosphates, sulfates, and carboxylates on cellular components (Rothbard et al. 2004; Sakai et al. 2005). In an effort to deliver a therapeutic peptide sequence derived from the proline-rich domain of DOC-2/DAB2 for prostate cancer treatment, we found out a polyarginine peptide (NH_2GR_{11}) with an unexpectedly preferential uptake in several prostate cancer cell lines (Zhou et al. 2006), which initiated the work presented in this paper. Two experiments were designed to verify whether the uptake preference is a unique feature of NH_2GR_{11} and whether it displays similar uptake specificity to prostate cancer in vivo. One was performed with three oligoarginines differing in the number of the repeating arginine units ($n = 9$, 11, and 13), which were labeled with a fluorescent dye (FITC: fluorescein isothiocyanate). NH_2GR_{11} was found with significantly higher uptake than NH_2GR_9 and NH_2GR_{13} in four human prostate cancer cell lines and in both normal and prostate cancer-bearing mouse models. Subsequently, a comparative PET-CT imaging study using prostate and lung cancer xenograft mouse models was carried out to test the specificity of using NH_2GR_{11} to image prostate cancer in vivo when labeled with ^{64}Cu ($t_{1/2} = 12.7$ h; β^+: 0.653 meV, 17.4%), a positron emitter. Our preliminary results demonstrate the potential of NH_2GR_{11} to be developed as a specific imaging probe for the detection of prostate cancer metastases.

Materials and methods

Chemical reagents and instrument

All chemicals were of reagent grade and used as received unless otherwise noted. FITC-$NHGR_9$, FITC-$NHGR_{11}$, FITC-$NHGR_{13}$, and DOTA-$NHGR_{11}$ (DOTA: 1,4,7,10-tetraazacyclododecane-1,4,7,10-tetraacetic acid) were synthesized by the Peptide Synthesis Laboratory of the University of Texas Southwestern Medical Center (Dallas, TX). Copper-64 chloride in 0.1 N HCl was purchased from the University of Wisconsin-Madison. Milli-Q water (18 MΩ cm) was obtained from a Millipore Gradient Milli-Q water system (Billerica, MA). All aqueous solutions were prepared with Milli-Q water. Light C-18 Sep-Pak cartridges were purchased from Waters (Milford, MA). Instant thin-layer chromatography (ITLC-SG) plates were purchased from Pall Life Sciences (East Hills, NY).

MALDI-TOF mass spectra were collected on a Voyager-DE™ PRO Biospectrometry Workstation (Applied Biosystems, Foster City, CA). Small animal PET-CT imaging studies were performed on a Siemens Inveon PET-CT Multimodality System (Siemens Medical Solutions Inc., Knoxville, TN).

Cell culture and animal models

All the cell lines used in this work (LNCaP, PZ-HPV-7, DU145, PC3, and H2009) were obtained from the American Type Culture Collection (ATCC, Manassas, VA). Both LNCaP and PC3 cell lines were cultured in T-media (Invitrogen Corporation, Carlsbad, CA) supplemented with 5% FBS and 1× penicillin/streptomycin. PZ-HPV-7 (an immortalized normal prostate epithelial cell line) and DU145 cell lines were maintained in PrEGM medium (Lonza, Walkersville, MD) and RPMI1640 medium (ThermoFisher Scientific, US) supplemented with 10% FBS and 1× penicillin/streptomycin, respectively. The H2009, a non-small lung cancer, cell line was cultured in RPMI1640 medium supplemented with 5% FBS. All the cell lines were cultured at 37°C in an atmosphere of 5% CO_2 and passaged at 75% confluence.

All animal studies were performed in compliance with guidelines set by the UT Southwestern Institutional Animal Care and Use Committee. Male nu/nu nude mice (5–7 weeks of age) were purchased from Harlan (Indianapolis, IN), and male SCID mice (6–8 weeks of age) were purchased from the UT Southwestern mouse-breeding core (Wakeland Colony). To establish the PC3 tumor xenograft mouse model, PC3 cell suspension was mixed 1:1 with Matrigel (BD Biosciences, Bedford, MA) and then injected subcutaneously (2×10^6 cells per site, injection volume 100 μL) into both flanks of animals. For the H2009 tumor

model, the cell suspension was injected subcutaneously (1×10^6 cells per site, injection volume 100 μL) into the back of both shoulders of SCID mice. After injection, the animals were monitored three times a week by general observations. Small PET-CT imaging was performed when the tumors become palpable.

In vitro cell uptake and subcellular localization

To determine the uptake efficiency of CPPs, 1×10^4 cells per well were seeded in 12-well plates and allowed to grow for 24 h. Then a FITC-tagged CCP (5 μM) was added and incubated with cells for 30 min. After removal of the medium, the cells were treated with Tryphan Blue (0.4% w/v, Mediatech, Inc., Herndon, VA) to quench the extracellular fluorescence and washed three times with cold PBS. The cells were then lysed with Tris Buffer (50 mM Tris–HCl, pH 7.5, 150 mM NaCl, 5 mM EDTA, 1% Triton X-100). The fluorescence intensity was measured by SpectraMax M5 (Molecular Devices, Sunnyvale, CA) with an excitation wavelength of 490 nm, an emission wavelength of 530 nm, and a cutoff wavelength of 515 nm. The protein concentration in each well was determined using a BCA protein assay kit (Pierce, Rockford, IL). The uptake efficiency of each CPP was determined by normalizing the fluorescence intensity with the protein concentration and the relative uptake was calculated as compared to that of FITC-$NHGR_{11}$. To determine the subcellular localization of a CPP, after 30 min incubation, the cells were fixed with 4% paraformaldehyde in PBS buffer and then counterstained with 1 μg/mL DAPI (Sigma, St. Louis, MO). Each sample was examined under a fluorescence microscope.

Preparation of ^{64}Cu-DOTA-$NHGR_{11}$

To a 1.5 mL vial containing 10 μg DOTA-$NHGR_{11}$ in 200 μL of 0.4 M NH_4OAc solution (pH 6.5), 2–3 mCi of ^{64}Cu in 0.1 M HCl was added. The reaction mixture was vortexed and then incubated at 37°C. After 30-min incubation, 5 μL of 5 mM diethylenetriaminepentaacetic acid (DTPA) was added and the reaction mixture was incubated at room temperature for 5 min. The separation of ^{64}Cu-DOTA-$NHGR_{11}$ from ^{64}Cu-DTPA was carried out by passing the reaction mixture through a light C-18 Sep-Pak cartridge. After three times of washings with PBS, the product was eluted with 80% ethanol solution. Radio-TLC analysis was performed on a Rita Star Radioisotope TLC Analyzer (Straubenhardt, Germany) to monitor the radiolabeling reaction using ITLC paper as the plate and 10 mM PBS as the mobile phase. High performance liquid chromatography (HPLC) analysis was conducted to determine the radiochemical purity of the products using a Waters 600 Multisolvent Delivery System equipped with a Waters 2996 Photodiode Array (PDA) detector and an in-line Shell Jr. 2000 radio-detector (Fredericksburg, VA) on a Waters Xterra column (150 × 4.6 mm, 5 μm). The mobile phase was H_2O with 0.1% TFA (solvent A) and acetonitrile with 0.1% TFA (solvent B). The gradient was 5–20% B in 0–5 min and 20–40% B in 5–25 min at 1.0 mL/min flow rate.

The cold reference of ^{nat}Cu-DOTA-$NHGR_{11}$ was prepared by reacting 1 mg (0.46 μmol) of DOTA-$NHGR_{11}$ with 62 μg (0.46 μmol) of $CuCl_2$ in 1 mL of 0.4 M NH_4OAc solution at 37°C for 1 h. The product was purified by HPLC using the same condition described above and characterized by MALDI-Mass (MALDI-TOF/MS: 2242.1 [$M + H^+$]). The fraction corresponding to ^{nat}Cu-DOTA-$NHGR_{11}$ was lyophilized and stored for use as cold standard.

Biodistribution and pharmacokinetic studies

The biodistribution studies were performed in control and PC3 tumor-bearing male nu/nu nude mice. Each mouse was injected intraperitoneally with a FITC-tagged CPP at a dose of 5 nmol/g of body weight. The animals were killed at 24 h post-injection (p.i.) and the organs of interest [prostate, seminal vesicle (SV), coagulation gland (CG), testis, liver, spleen, kidneys, muscle, lung, brain, and tumor] were excised, weighed, and measured by the fluorescence reader. The relative FITC intensity of each CPP was calculated as fluorescence intensity per gram of tissue weight.

Pharmacokinetic parameters were estimated by a two-compartment model using normal male nu/nu nude mice. Blood (~5 μL) was drawn from the retro-orbital sinus of the mice at 5, 10, 20, and 40 min after the tail vein injection of ^{64}Cu-DOTA-$NHGR_{11}$, and then counted on a γ-counter.

Small animal PET/CT imaging

When the tumor size reached the range of 50–300 mm^3, the tumor-bearing mice were randomized for the PET-CT imaging with ^{64}Cu-DOTA-$NHGR_{11}$. The injected dose was 3.7 MBq of ^{64}Cu-activity in 100 μL of PBS, while the injected molar amount of NH_2GR_{11} was maintained at the same level by decay correction.

Ten minutes prior to imaging, the animal was anesthetized using 3% isofluorane at room temperature until stable vitals were established. Once the animal was sedated, it was placed onto the imaging bed under 2% isofluorane anesthesia for the duration of the imaging. The CT imaging was acquired at 80 kV and 500 μA with a focal spot of 58 μm. The total rotation of the gantry was 360° with 360 rotation steps obtained at an exposure time of approximately 235 ms/frame. The images were attained using a CCD readout of 4,096 × 3,098 with a bin factor of 4 and

an average frame of 1. Under low magnification, the effective pixel size was 103.03 μm. Total CT scan time was approximately 6 min. CT images were reconstructed with a down sample factor of 2 using Cobra Reconstruction Software. The PET imaging was performed directly after the acquisition of CT data. The PET tracer was injected intravenously via the tail vein. Static PET scans were performed at 1, 4, and 24 h p.i. for 15 min. PET images at 1, 4, and 24 h p.i. were reconstructed using Fourier Rebinning and Ordered Subsets Expectation Maximization 3D (OSEM3D) algorithm. Reconstructed CT and PET images were fused and analyzed using the Siemens Inveon Research Workplace (IRW) software. For quantification, regions of interest were placed in the areas expressing the highest radiotracer activity as determined by visual inspection. The tissues examined include the left and right tumors, heart, liver, lung, kidneys, and muscle. The resulting quantitative data were expressed as percent injected dose per gram of tissue (%ID/g).

Statistical analysis

Quantitative data were expressed as mean ± SD and then compared using one-way analysis of variance and Student's t test. P values <0.05 were considered statistically significant.

Results

In vitro cell uptake and subcellular localization

The oligoarginine length effect on the cell uptake efficiency was evaluated using FITC-$NHGR_9$, FITC-$NHGR_{11}$ and FITC-$NHGR_{13}$ in four different human prostate cell lines: PZ-HPV-7, LNCaP, PC3, and DU145. For comparison, the uptake of FITC-$NHGR_{11}$ in LNCaP is set at 1.0. As shown in Fig. 1a, after 30 min incubation, FITC-$NHGR_{11}$ displayed much higher uptake efficiency

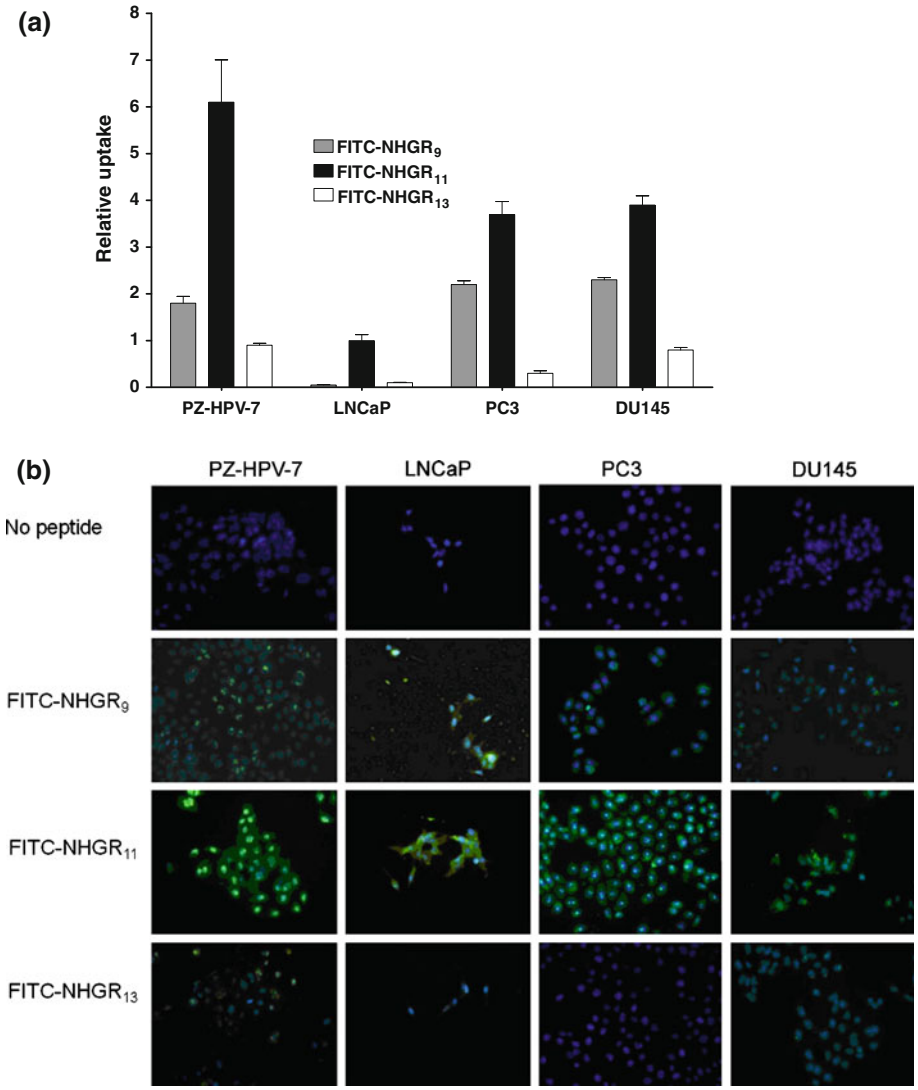

Fig. 1 Uptake of FITC-$NHGR_9$, FITC-$NHGR_{11}$, and FITC-$NHGR_{13}$ by prostate cells (PZ-HPV-7, LNCaP, PC3 and DU145). **a** FITC-$NHGR_9$, FITC-NH_2GR_{11}, and FITC-NH_2GR_{13} were incubated with cells for 30 min before cell harvesting. Relative FITC intensity was determined by normalizing fluorescence intensity with its protein content and presented as relative level compared to uptake of FITC-$NHGR_{11}$ in LNCaP. *Columns* mean in triplicate, *bars* SD. All the experiments were repeated at least twice. **b** Cells were incubated with 5 μmol/L of the indicated peptide for 30 min. After fixation, cells were counterstained with DAPI. The cellular distribution of each peptide was visualized with a fluorescence microscope

than FITC-$NHGR_9$ and FITC-$NHGR_{13}$ ($P < 0.005$) in all the four cell lines indicating that the intracellular uptake of oligoarginines is greatly affected by the number of the repeating guanidino moiety. Of the three FITC-tagged oligoarginines, FITC-$NHGR_{13}$ showed the lowest uptake in three of the tested cell lines (PZ-HPV-7, PC3, and DU145). In PC3 and DU145, FITC-$NHGR_9$ displayed appreciable uptake values, which are 63 and 65% of that of FITC-$NHGR_{11}$, respectively. Overall, the PZ-HPV-7 and LNCaP cell lines exhibited highly selective internalization of oligoarginines varying with the peptide length.

The subcellular localization of FITC-$NHGR_9$, FITC-$NHGR_{11}$, and FITC-$NHGR_{13}$ in the prostate cancer cell lines was shown in Fig. 1b. Apparently, FITC-$NHGR_{11}$ exhibited a higher fluorescent intensity in all the cell lines. The majority of FITC-$NHGR_{11}$ was localized in the cytosol, while in PZ-HPV-7 and PC3 cell lines, nuclear staining with FITC-$NHGR_{11}$ was also seen. Both FITC-$NHGR_9$ and FITC-$NHGR_{13}$ showed significantly lower fluorescent intensity than FITC-$NHGR_{11}$ in all four tested cell lines, which is consistent with the cell uptake results. Taken together, these data demonstrate the high efficiency and amino acid length-dependent uptake of FITC-$NHGR_{11}$ in various prostate cell lines, which has made FITC-$NHGR_{11}$ as a unique probe for detecting prostate cancer.

Preparation of ^{64}Cu-DOTA-$NHGR_{11}$

To label NH_2GR_{11} with ^{64}Cu, a commonly used bifunctional chelator, DOTA was conjugated to the N terminus of the peptide. The conjugate, DOTA-$NHGR_{11}$, was labeled with ^{64}Cu by incubating with $^{64}Cu^{2+}$ in 0.4 M NH_4OAc buffer (pH 6.5) at 37°C for 30 min. Non-specifically bound ^{64}Cu was removed in the form of ^{64}Cu-DTPA at the end of the radiolabling procedure. The radiolabeling reaction was monitored by radio-TLC analysis, in which the reaction mixture was sampled on an instant TLC plate that was then developed in PBS buffer. Under the TLC conditions, ^{64}Cu-DOTA-$NHGR_{11}$ stayed at the origin, while ^{64}Cu-DTPA moved to the solvent front. The radiochemical yield was >90% when 10 μg of the DOTA conjugate was used to label 2–3 mCi of ^{64}Cu. The ^{64}Cu-DTPA was removed by passing the reaction mixture through a light C18 Sep-Pak cartridge and three times of washing with PBS. The product, ^{64}Cu-DOTA-$NHGR_{11}$, could then be efficiently eluted with 80% of ethanol. The radiochemical purity of ^{64}Cu-DOTA-$NHGR_{11}$ was nearly 100% after the Sep-Pak purification as determined by radio-ITLC and radio-HPLC.

To confirm the identity of the labeled product, ^{nat}Cu-DOTA-$NHGR_{11}$ was prepared and used as a reference standard. Both ^{64}Cu-DOTA-$NHGR_{11}$ and ^{nat}Cu-DOTA-$NHGR_{11}$ showed a single peak on HPLC (^{64}Cu-DOTA-$NHGR_{11}$: radioactivity detector; ^{nat}Cu-DOTA-$NHGR_{11}$: PDA UV detector) with the same retention time within 14–15 min.

Biodistribution and in vivo pharmacokinetics

The tissue distribution of FITC-$NHGR_9$, FITC-$NHGR_{11}$, and FITC-$NHGR_{13}$ was conducted in control and PC-3 tumor-bearing nude mice. The biodistribution data are presented in Figs. 2 and 3, respectively. For comparison, the uptake value of FITC-$NHGR_9$ in the prostate is set at 1.0 in Fig. 2. Compared to FITC-$NHGR_9$ and FITC-$NHGR_{13}$, FITC-$NHGR_{11}$ clearly showed preferential accumulation in the prostate tissue as measured by the uptake ratios of the prostate to other organs. As shown in Fig. 3, FITC-$NHGR_{11}$ displayed high relative uptake values in both prostate tissue and prostate tumor. Impressively, the uptake ratios of tumor to muscle and prostate to muscle were 3.8 and 8.7, respectively. In addition, FITC-$NHGR_{11}$ showed low uptake in the major clearance organs (e.g. liver, spleen, and kidneys).

Given the limited capability of fluorescence imaging quantification for in vivo evaluations, the in vivo pharmacokinetics of NH_2GR_{11} was evaluated using ^{64}Cu-DOTA-$NHGR_{11}$ in normal mice based on a two-compartment model. Its half-life in the blood (the primary compartment) was 10.7 min; and the elimination half-life from other organs (the secondary compartment) was 17.2 h.

Small animal PET-CT imaging

The comparative small animal imaging evaluation of ^{64}Cu-DOTA-$NHGR_{11}$ was performed using PC3 and H2009 tumor-bearing SCID mice, which were injected with a

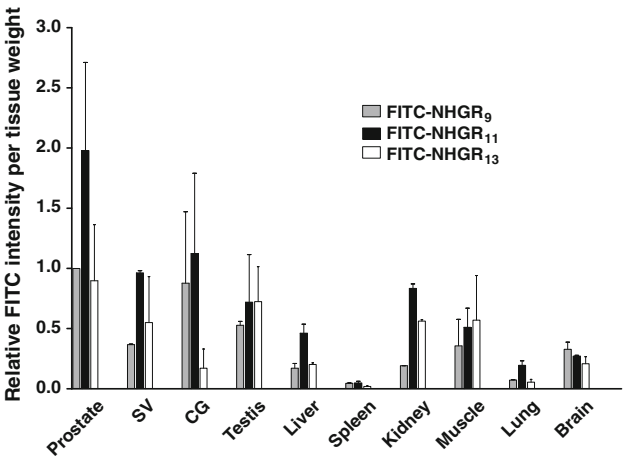

Fig. 2 Biodistribution of FITC-$NHGR_9$, FITC-$NHGR_{11}$, and FITC-$NHGR_{13}$ in normal male nu/nu nude mice at 24 h p.i. ($n = 3$). *SV* seminal vesicle and *CG* coagulation gland

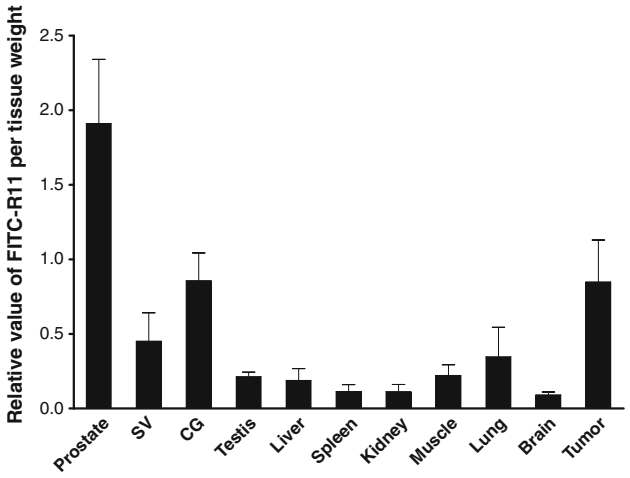

Fig. 3 Biodistribution of FITC-$NHGR_{11}$ in PC3 tumor-bearing mice at 24 h p.i. ($n = 4$)

similar amount of peptide with respect to the volume of tumor as calculated based on the specificity radioactivity of ^{64}Cu-DOTA-$NHGR_{11}$. The PET-CT imaging acquisition was conducted at 1, 4, and 24 h p.i. ($n = 3$ at each time point). The representative PET-CT images (transaxial) are presented in Fig. 4. Clearly the PC3 tumors on both flanks were visualized by ^{64}Cu-DOTA-$NHGR_{11}$ on PET images at 1, 4 and 24 h p.i. In contrast, the H2009 tumors were only visible at 1 and 4 h with much lower signal intensity on PET as compared to the PC3 tumors; at 24 h p.i., they became not detectable.

The PET images were quantitatively analyzed by the Siemens Inveon Research Workplace (IRW) software. Summarized in Table 1 are the uptake values of ^{64}Cu-DOTA-$NHGR_{11}$ in the regions of interest [tumors (left and right), heart, liver, lung, kidney (left), and muscle] obtained from the imaging quantification. Not surprisingly, ^{64}Cu-DOTA-$NHGR_{11}$ showed nearly identical uptake values in the right and left tumors. The accumulation level of ^{64}Cu-DOTA-$NHGR_{11}$ in the PC3 tumors remained steady out to 24 h p.i. (1.17 ± 0.19%ID/g at 1 h p.i.; 0.91 ± 0.32%ID/g at 4 h; 24 h 0.82 ± 0.24%ID/g at 24 h), whereas its uptake in the H2009 tumors was significantly lower ($P < 0.02$) and showed an appreciable trend of decreases over time (0.81 ± 0.07%ID/g at 1 h p.i.; 0.47 ± 0.12%ID/g at 4 h; 24 h 0.33 ± 0.05%ID/g at 24 h). Impressively, the uptake ratios of ^{64}Cu-DOTA-$NHGR_{11}$ in PC3 tumor versus muscle at 1, 4, and 24 h p.i. were 5.06 ± 0.96, 4.87 ± 1.29, and 10.41 ± 6.07, respectively. In other organs, ^{64}Cu-DOTA-$NHGR_{11}$ exhibited a very similar distribution pattern in both tumor-bearing mouse models.

Discussion

In spite of the extensive utilization of arginine-rich CPPs for intracellular delivery of a broad range of bioactive materials, the internalization mechanisms of CPPs are still under investigation. It has been reported that a slight structural alteration might lead to significant changes of the CPP internalization mechanisms or subcellular localization, which can thereby considerably affect its internalization efficiency and the bioavailability of its cargos (Nakase et al. 2008). Internalization selectivity of CPPs into specific cells or organs is highly desirable for efficient target delivery of therapeutics in order to minimize the side effects on non-target organs. This selectivity can be obviously imparted by attaching a targeting molecule to the CPP-cargo conjugate, although it adds complexity to the overall construct. From screening of various CPPs for the potential candidate of delivery vehicle in prostate cancer, we have reported that an arginine-rich CPP exhibits a high efficiency of intracellular uptake in vitro (Zhou et al. 2006). In 2007, Elson-Schwab et al. (2007) reported that the delivery of arginine-rich CPPs at nanomolar transporter concentrations was completely mediated by the membrane-associated heparan sulfate proteoglycans (HSPG). Given the fact that the expression level of HSPG varies with cell type (Sasisekharan et al. 2002; Sanderson et al. 2004), it is not surprising that CPPs with certain structure or sequence may display cell or organ specificity to some extent. Indeed, the fact that the negatively charged heparan

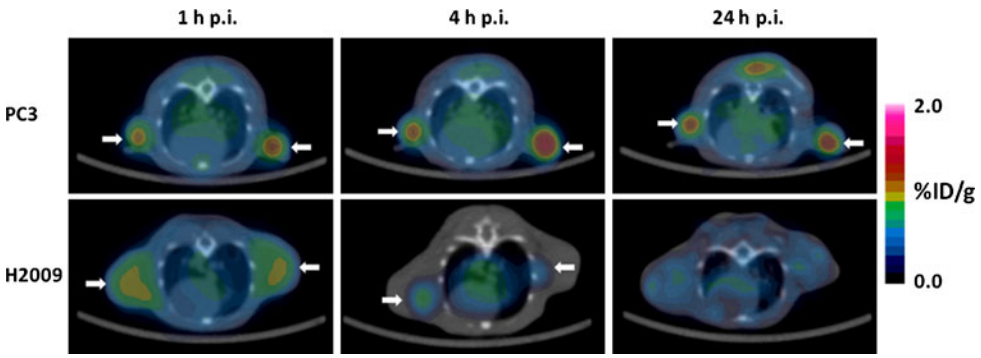

Fig. 4 Representative transaxial PET-CT images of ^{64}Cu-DOTA-$NHGR_{11}$ in PC3 and H2009 tumor-bearing mice at 1, 4, and 24 h p.i. ($n = 3$). The *white arrows* indicate tumors

Table 1 PET quantification data of ^{64}Cu-DOTA-NHGR$_{11}$ in PC3 and H2009 tumor-bearing mice at 1, 4, and 24 h p.i.

%ID/g	PC3 tumor model			H2009 tumor model		
	1 h	4 h	24 h	1 h	4 h	24 h
Tumor	1.17 ± 0.19**	0.91 ± 0.32*	0.82 ± 0.24***	0.81 ± 0.07**	0.47 ± 0.12*	0.33 ± 0.05***
Heart	0.58 ± 0.06	0.52 ± 0.03	0.40 ± 0.06	0.72 ± 0.05	0.43 ± 0.13	0.39 ± 0.03
Liver	9.13 ± 1.75	7.95 ± 1.91	5.03 ± 1.17	8.13 ± 0.12	7.63 ± 0.31	7.20 ± 0.46
Lung	0.59 ± 0.07	0.62 ± 0.10	0.43 ± 0.08	0.55 ± 0.04	0.27 ± 0.05	0.31 ± 0.09
Kidneys	3.93 ± 0.21	3.40 ± 0.00	1.73 ± 0.06	4.27 ± 0.15	4.33 ± 0.35	2.10 ± 0.26
Muscle	0.24 ± 0.06	0.18 ± 0.03	0.09 ± 0.05	0.24 ± 0.03	0.15 ± 0.09	0.09 ± 0.01

Data are presented as %ID/g ± SD ($n = 3$; *$P < 0.02$; **$P < 0.002$; ***$P < 0.001$)

sulfates on HSPG can form divalent hydrogen-bonds with the guanidino groups (Nakase et al. 2008) may explain the role of HSPG in the internalization of arginine-rich CPPs.

Heparan sulfate proteoglycans consist of a diverse family of glycosaminoglycan-bearing protein cores including the syndecans and perlecan (Kirn-Safran et al. 2009). Recently, Datta et al. (2006) reported that perlecan, also called HSPG-2, is highly expressed in various prostate cancer cell lines including LNCaP, PC3, and DU145, and the cell growth is inhibited by silencing the expression of perlecan. In addition, the level of perlecan in prostate cancer tissues was found in good correlation with the Gleason score and rapid cell proliferation. Similarly, syndecan-1, a cell membrane-bound HSPG, was reported with a great overexpression during the androgen-independent progression of prostate cancer in a mouse model (Alexander et al. 2000) and the androgen-independent prostate cancer cell lines, such as PC3 and DU145 (Chen et al. 2004a, b).

The preferential uptake of NH_2GR_{11} that we observed in various prostate cancer cell lines could be reasonably explained by the upregulated expression of HSPG in prostate tissues or cancer cells. This prompted us to speculate the potential application of NH_2GR_{11} as PET imaging probe for the diagnosis of prostate cancer, while the detailed mechanism of this specific uptake may take years of research to reveal. It is noteworthy that other CPPs with different sequences or lengths may exhibit similar or even better prostate tissue uptake specificity. Given the high uptake of NH_2GR_{11} was also observed in the normal prostate tissue (Figs. 2, 3), we believe that the NH_2GR_{11}-based PET imaging probes will be more suitable for the detection of distant prostate cancer metastases such as lymph node and bone metastases rather than primary prostate tumor. Indeed, there has been a postulation that the bone extracellular matrix is a perlecan-rich site, which explains why prostate cancer preferentially metastasizes to the bone (Datta et al. 2006).

In the present work, we first evaluated the length effect on the internalization efficiency using three FITC-tagged oligoarginines differing in the number of repeating arginine units in hope for an optimal length for the following evaluations. The in vitro cell uptake and subcellular localization experiments were performed in four different prostate cell lines. The result was what we anticipated to some extent. The CPP with 11 arginine-repeating units, NH_2GR_{11}, unequivocally demonstrated its superiority over other two CPPs with either shorter or longer length in term of absolute cell uptake and internalization efficiency (Fig. 1). As shown in Fig. 1b, NH_2GR_{11} was primarily presented in the cytosol after being internalized.

Given the in vitro result, we proceeded to evaluate whether NH_2GR_{11} could maintain the superior properties in normal nude mice as compared to NH_2GR_9 and NH_2GR_{13}. As measured by the uptake ratios of the prostate to other organs, a clear preferential accumulation in the prostate tissue was observed for FITC-NHGR$_{11}$ but not for either FITC-NHGR$_9$ or FITC-NHGR$_{13}$. This overall in vivo uptake result of the three FITC-tagged peptides is similar to the in vitro result, indicating that the biologic activity of these CPPs remains quite consistent under the environment of different tissue types. Nevertheless, this high uptake in normal prostate tissue exhibited by FITC-NHGR$_{11}$ precludes NH_2GR_{11} from being considered as imaging probes for primary prostate cancer detection. However, it can be well suited for the detection of distant prostate cancer metastases. As such we further evaluated the biodistribution profile of FITC-NHGR$_{11}$ in PC3 tumor-bearing animal with the tumor distant from the normal prostate (Fig. 3). In addition to the expected high uptake in the prostate, FITC-NHGR$_{11}$ showed elevated accumulation in the PC3 tumor, which serves as an analogic model of distant prostate cancer metastasis.

The in vivo pharmacokinetics of NH_2GR_{11} evaluated with ^{64}Cu-DOTA-NHGR$_{11}$ in normal mice showed that the CPP was cleared from the blood rapidly with a half-life of 10.7 min, but its elimination half-life from other organs

(the secondary compartment) was rather long (17.2 h). This was why we chose ^{64}Cu ($t_{1/2}$: 12.7 h) instead of ^{18}F ($t_{1/2}$: 110 min) for the PET application of NH_2GR_{11}.

The labeling of DOTA-$NHGR_{11}$ with ^{64}Cu was straightforward. The radiochemical yields were reasonably high. After the purification by a light C18 Sep-Pak cartridge, the radiochemical purity of ^{64}Cu-DOTA-$NHGR_{11}$ was nearly 100% as determined by a reverse phase HPLC method. The specific radioactivity of ^{64}Cu-DOTA-$NHGR_{11}$ was 11 GBq/μmol.

With the goal to develop NH_2GR_{11} for specific PET imaging of prostate cancer metastases, we designed and performed a comparative PET-CT imaging experiment using PC3 and H2009 tumor-bearing mouse models. However, due to the availability of ^{64}Cu and the tumor-growth rate difference between PC3 and H2009, the tumor sizes of PC3 and H2009 could not be ideally matched for this preliminary evaluation. The PC3 tumors were around 100 mm^3 at the time of PET-CT imaging, while the H2009 tumor size was in the range of 100–300 mm^3. However, the PC3 tumors were clearly visualized with ^{64}Cu-DOTA-$NHGR_{11}$ at 1, 4, and 24 h p.i., while the H2009 tumors became invisible on PET images after 4 h p.i. The PET imaging quantification further confirmed that the absolute uptake of ^{64}Cu-DOTA-$NHGR_{11}$ in the PC3 tumors was significantly higher than in the H2009 tumors throughout the imaging study, indicating the desired imaging specificity of ^{64}Cu-DOTA-$NHGR_{11}$. The slow clearance of ^{64}Cu-DOTA-$NHGR_{11}$ from the PC3 tumors likely reflects the fact that the radiotracer had been internalized into the tumor cells within 1 h p.i., while the significant clearance of ^{64}Cu-DOTA-$NHGR_{11}$ from the H2009 tumors probably indicates that the radiotracer could not be efficiently internalized into the lung cancer cells. Intriguingly, there are reports that the syndecan-1 expression is lost in lung cancer (Nackaerts et al. 1997; Chen et al. 2004a, b).

It is noteworthy that the biodistribution profiles of NH_2GR_{11} obtained from FITC-$NHGR_{11}$ and ^{64}Cu-DOTA-$NHGR_{11}$ (Fig. 2; Table 1) are not in good agreement with regard to the uptake values in the liver and kidneys. While the discrepancies might be caused by the different administration routes of FITC-$NHGR_{11}$ and ^{64}Cu-DOTA-$NHGR_{11}$, the high accumulation of ^{64}Cu-DOTA-$NHGR_{11}$ in the liver could be partially resulted from the dislocation of ^{64}Cu from the DOTA moiety (Boswell et al. 2004). To circumvent this in vivo stability problem, in our future evaluations of NH_2GR_{11}, we will replace the DOTA moiety with a cross-bridged tetraazamacrocyclic bifunctional chelator (CB-TE2A: 4,11-bis(carboxymethyl)-1,4,8,11-tetraazabicyclo[6.6.2]hexadecane) whose ^{64}Cu-complex has been shown with strong resistance to the in vivo transchelation of ^{64}Cu (Sun et al. 2002).

Conclusions

We have demonstrated the potential of using $NHGR_{11}$ to develop specific PET imaging probes for distant prostate cancer metastases by both in vitro and in vivo evaluations performed with FITC-$NHGR_{11}$ and ^{64}Cu-DOTA-$NHGR_{11}$. Further mechanistic elucidation of the cell uptake and internalization of arginine-rich CPPs would facilitate the development of this unique group of molecules for targeted molecular imaging and drug delivery.

Acknowledgments This work was partially supported by the Prostate Cancer Research Program of the United States Army Medical Research and Materiel Command (W81XWH-08-1-0305 and W81XWH-04-1-0222), a Clinical Innovator Award from the Flight Attendant Medical Research Institute, and a small animal imaging research program grant (SAIRP) from the National Institute of Cancer (U24 CA126608). The authors acknowledge the generous support of a private donor that allowed the purchase of the Siemens Inveon PET-CT Multi-modality System.

References

Albrecht S, Buchegger F, Soloviev D, Zaidi H, Vees H, Khan HG, Keller A, Bischof Delaloye A, Ratib O, Miralbell R (2007) (11)C-acetate PET in the early evaluation of prostate cancer recurrence. Eur J Nucl Med Mol Imaging 34(2):185–196

Alexander CM, Reichsman F, Hinkes MT, Lincecum J, Becker KA, Cumberledge S, Bernfield M (2000) Syndecan-1 is required for Wnt-1-induced mammary tumorigenesis in mice. Nat Genet 25(3):329–332

Beheshti M, Langsteger W, Fogelman I (2009) Prostate cancer: role of SPECT and PET in imaging bone metastases. Semin Nucl Med 39(6):396–407

Boswell CA, Sun XK, Niu WJ, Weisman GR, Wong EH, Rheingold AL, Anderson CJ (2004) Comparative in vivo stability of copper-64-labeled cross-bridged and conventional tetraazamacrocyclic complexes. J Med Chem 47(6):1465–1474

Bouchelouche K, Capala J, Oehr P (2009) Positron emission tomography/computed tomography and radioimmunotherapy of prostate cancer. Curr Opin Oncol 21(5):469–474

Bucci M, Gratton JP, Rudic RD, Acevedo L, Roviezzo F, Cirino G, Sessa WC (2000) In vivo delivery of the caveolin-1 scaffolding domain inhibits nitric oxide synthesis and reduces inflammation. Nat Med 6(12):1362–1367

Chen D, Adenekan B, Chen L, Vaughan ED, Gerald W, Feng Z, Knudsen BS (2004a) Syndecan-1 expression in locally invasive and metastatic prostate cancer. Urology 63(2):402–407

Chen XY, Park R, Hou YP, Tohme M, Shahinian AH, Bading JR, Conti PS (2004b) MicroPET and autoradiographic imaging of GRP receptor expression with Cu-64-DOTA-[Lys(3)]bombesin in human prostate adenocarcinoma xenografts. J Nucl Med 45(8):1390–1397

Datta MW, Hernandez AM, Schlicht MJ, Kahler AJ, DeGueme AM, Dhir R, Shah RB, Farach-Carson C, Barrett A, Datta S (2006) Perlecan, a candidate gene for the CAPB locus, regulates prostate cancer cell growth via the Sonic Hedgehog pathway. Mol Cancer 5:9

Elson-Schwab L, Garner OB, Schuksz M, Crawford BE, Esko JD, Tor Y (2007) Guanidinylated neomycin delivers large, bioactive

cargo into cells through a heparan sulfate-dependent pathway. J Biol Chem 282(18):13585–13591

Emonds KM, Swinnen JV, Mortelmans L, Mottaghy FM (2009) Molecular imaging of prostate cancer. Methods 48(2):193–199

Etchebehere ECSC, Macapinlac HA, Gonen M, Humm J, Yeung HWD, Akhurst T, Scher HI, Larson SM (2002) Qualitative and quantitative comparison between images obtained with filtered back projection and iterative reconstruction in prostate cancer lesions on F-18-FDG PET. Q J Nucl Med 46(2):122–130

Fogelman I, Cook G, Israel O, Van der Wall H (2005) Positron emission tomography and bone metastases. Semin Nucl Med 35(2):135–142

Gambhir SS (2002) Molecular imaging of cancer with positron emission tomography. Nat Rev Cancer 2(9):683–693

Giovacchini G, Gajate AM, Messa C, Fazio F (2008) Increased C-11 choline uptake in pagetic bone in a patient with coexisting skeletal metastases from prostate cancer. Clin Nucl Med 33(11):797–798

Gratton JP, Yu J, Griffith JW, Babbitt RW, Scotland RS, Hickey R, Giordano FJ, Sessa WC (2003) Cell-permeable peptides improve cellular uptake and therapeutic gene delivery of replication-deficient viruses in cells and in vivo. Nat Med 9(3):357–362

Hara T, Kosaka N, Kishi H (1998) PET imaging of prostate cancer using carbon-11-choline. J Nucl Med 39(6):990–995

Kirn-Safran C, Farach-Carson MC, Carson DD (2009) Multifunctionality of extracellular and cell surface heparan sulfate proteoglycans. Cell Mol Life Sci 66(21):3421–3434

Langsteger W, Heinisch M, Fogelman I (2006) The role of fluorodeoxyglucose, 18F-dihydroxyphenylalanine, 18F-choline, and 18F-fluoride in bone imaging with emphasis on prostate and breast. Semin Nucl Med 36(1):73–92

Larson SM, Morris M, Gunther I, Beattie B, Humm JL, Akhurst TA, Finn RD, Erdi Y, Pentlow K, Dyke J, Squire O, Bornmann W, McCarthy T, Welch M, Scher H (2004) Tumor localization of 16beta-18F-fluoro-5alpha-dihydrotestosterone versus 18F-FDG in patients with progressive, metastatic prostate cancer. J Nucl Med 45(3):366–373

Maeda T, Tateishi U, Komiyama M, Fujimoto H, Watanabe S, Terauchi T, Moriyama N, Arai Y, Sugimura K, Kakizoe T (2006) Distant metastasis of prostate cancer: early detection of recurrent tumor with dual-phase carbon-11 choline positron emission tomography/computed tomography in two cases. Jpn J Clin Oncol 36(9):598–601

Nackaerts K, Verbeken E, Deneffe G, Vanderschueren B, Demedts M, David G (1997) Heparan sulfate proteoglycan expression in human lung-cancer cells. Int J Cancer 74(3):335–345

Nakase I, Takeuchi T, Tanaka G, Futaki S (2008) Methodological and cellular aspects that govern the internalization mechanisms of arginine-rich cell-penetrating peptides. Adv Drug Deliver Rev 60(4–5):598–607

Oyama N, Miller TR, Dehdashti F, Kibel AS, Michalski JM, Fischer KC, Picus J, Siegel BA, Andriole GL, Welch MJ (2002) Carbon-11-acetate PET imaging of recurrent prostate cancer. J Urol 167(4):173–174

Oyama N, Ponde DE, Dence C, Kim J, Tai YC, Welch MJ (2004) Monitoring of therapy in androgen-dependent prostate tumor model by measuring tumor proliferation. J Nucl Med 45(3):519–525

Ponde DE, Dence CS, Oyama N, Kim J, Tai YC, Laforest R, Siegel BA, Welch MJ (2007) 18F-fluoroacetate: a potential acetate analog for prostate tumor imaging—in vivo evaluation of 18F-fluoroacetate versus 11C-acetate. J Nucl Med 48(3):420–428

Rogers BE, Bigott HM, McCarthy DW, Della Manna D, Kim J, Sharp TL, Welch MJ (2003) MicroPET imaging of a gastrin-releasing peptide receptor-positive tumor in a mouse model of human prostate cancer using a 64Cu-labeled bombesin analogue. Bioconjug Chem 14(4):756–763

Rothbard JB, Jessop TC, Lewis RS, Murray BA, Wender PA (2004) Role of membrane potential and hydrogen bonding in the mechanism of translocation of guanidinium-rich peptides into cells. J Am Chem Soc 126(31):9506–9507

Sakai N, Takeuchi T, Futaki S, Matile S (2005) Direct observation of anion-mediated translocation of fluorescent oligoarginine carriers into and across bulk liquid and anionic bilayer membranes. ChemBioChem 6(1):114–122

Sanderson RD, Yang Y, Suva LJ, Kelly T (2004) Heparan sulfate proteoglycans and heparanase-partners in osteolytic tumor growth and metastasis. Matrix Biol 23(6):341–352

Sasisekharan R, Shriver Z, Venkataraman G, Narayanasami U (2002) Roles of heparan-sulphate glycosaminoglycans in cancer. Nat Rev Cancer 2(7):521–528

Schuhmacher J, Zhang H, Doll J, Macke HR, Matys R, Hauser H, Henze M, Haberkorn U, Eisenhut M (2005) GRP receptor-targeted PET of a rat pancreas carcinoma xenograft in nude mice with a 68 Ga-labeled bombesin(6–14) analog. J Nucl Med 46(4):691–699

Shreve PD, Grossman HB, Gross MD, Wahl RL (1996) Metastatic prostate cancer: initial findings of PET with 2-deoxy-2-[F-18]fluoro-D-glucose. Radiology 199(3):751–756

Sun XK, Wuest M, Weisman GR, Wong EH, Reed DP, Boswell CA, Motekaitis R, Martell AE, Welch MJ, Anderson CJ (2002) Radiolabeling and in vivo behavior of copper-64-labeled cross-bridged cyclam ligands. J Med Chem 45(2):469–477

Vees H, Buchegger F, Albrecht S, Khan H, Husarik D, Zaidi H, Soloviev D, Hany TF, Miralbell R (2007) F-18-choline and/or C-11-acetate positron emission tomography: detection of residual or progressive subclinical disease at very low prostate-specific antigen values (<1 ng/mL) after radical prostatectomy. BJU Int 99(6):1415–1420

Yang YS, Zhang XZ, Xiong ZM, Chen XY (2006) Comparative in vitro and in vivo evaluation of two Cu-64-labeled bombesin analogs in a mouse model of human prostate adenocarcinoma. Nucl Med Biol 33(3):371–380

Zhang X, Cai W, Cao F, Schreibmann E, Wu Y, Wu JC, Xing L, Chen X (2006) 18F-labeled bombesin analogs for targeting GRP receptor-expressing prostate cancer. J Nucl Med 47(3):492–501

Zhou J, Fan J, Hsieh JT (2006) Inhibition of mitogen-elicited signal transduction and growth in prostate cancer with a small peptide derived from the functional domain of DOC-2/DAB2 delivered by a unique vehicle. Cancer Res 66(18):8954–8958